Electronic Supplementary Material (ESI) for Materials Chemistry Frontiers.

Supplementary Information:

Effect of H-bonding on Network Junction and Macroscopic Elastomer Properties in Photocured Polyacrylate Films

Bing Wu,[†,‡,§,*] Walter Chassé,[⊥] Andreas Heise,[§] Arno P. M. Kentgens,[‖] Dermot F. Brougham,[‡,*] Victor M. Litvinov[∏,*]

† Dutch-Belgian Beamline (DUBBLE), ESRF- The European Synchrotron Radiation Facility, CS 40220, 38043 Grenoble Cedex 9, France

‡ School of Chemistry, University College Dublin, Belfield, Dublin 4, Ireland

§ Department of Chemistry, Royal College of Surgeons in Ireland, 123 St. Stephen's Green, Dublin 2, Ireland

⊥ Institut für Physikalishe Chemie, University of Münster, Corrensstr. 28/30, 48149 Münster. Germany

‖ Institute for Molecules and Materials, Radboud University Nijmegen, Heyendaalsweg 135, 6525 AJ Nijmegen, The Netherlands

∏ V. Lit Consult, Gozewijnstraat 4, 6191WV, Beek, The Netherlands

S1. Structural Analyses of Networks

Detailed experimental settings and sample preparation procedures can be found in our previous publication.[1]

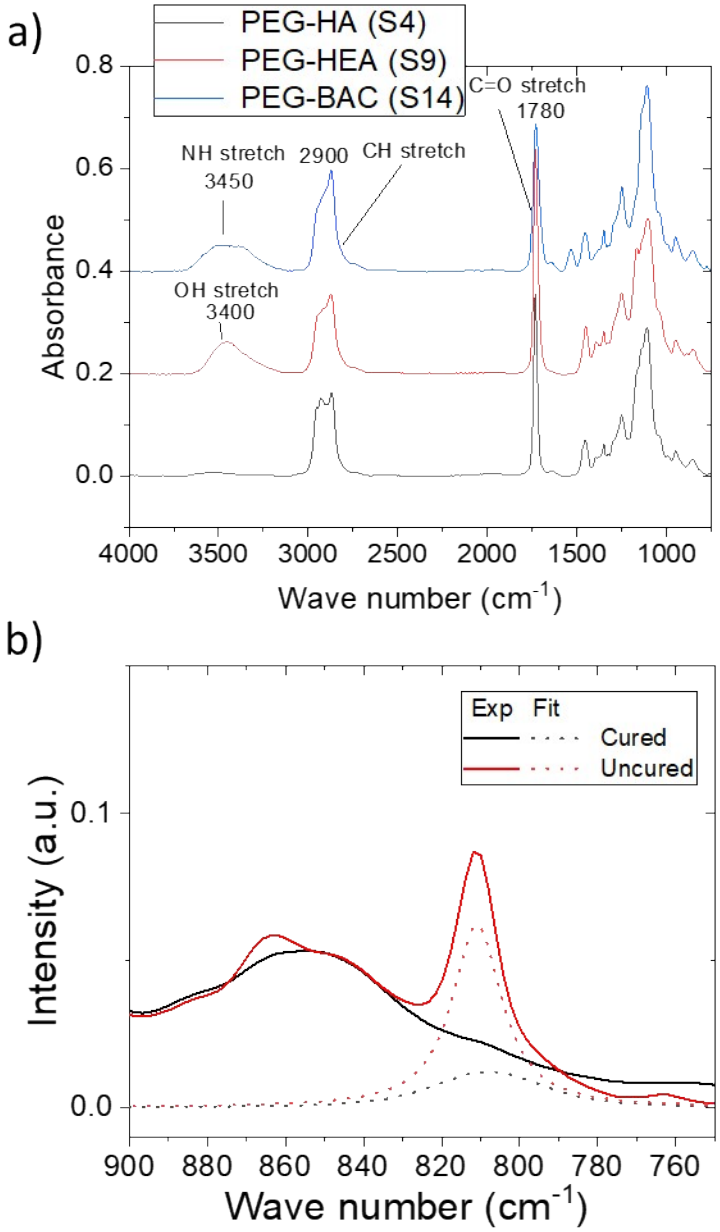

Figure S1 IR spectrum of a) sample PEG-HA (50w% HA), PEG-HEA (50w% HEA) and PEG-BAC (50w% BAC); b) acrylate C-H deformation band at 810 cm^{-1} for uncured and cured PEG-HEA sample (10wt% HEA).

Infrared analyses were carried out on Bruker Alpha-P FTIR spectrometer. As shown in **Fig. S1b**, 90% of the acrylates were cured during the photopolymerization process, while the solution state ^{1}H NMR for the extractable (Fig. S2) show less than 5 wt% acrylates raw materials were physically

entrapped inside the network after photocuring step. We have previously shown using ^{1}H NMR spectrum of the extracts from PEG-HA that oxygen inhibition reactions were insignificant, if they happened at all.[1] Finally, ^{13}C CPMAS NMR spectra (Figures S2-S4) imply the formation of fully cured networks with little defects.

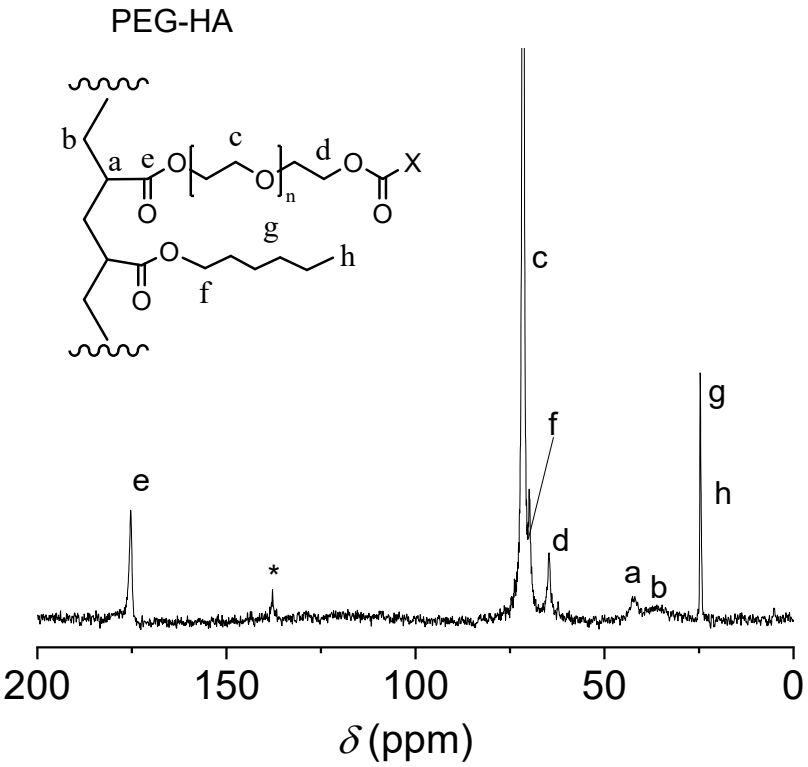

Figure S2. ^{13}C CP MAS NMR spectrum for cured PEG-HA network and its assignment. Rotor spinning speed 12 kHz, contact time 10 ms, recycle delay 5s. * represents uncured acrylate double-bond carbon species.

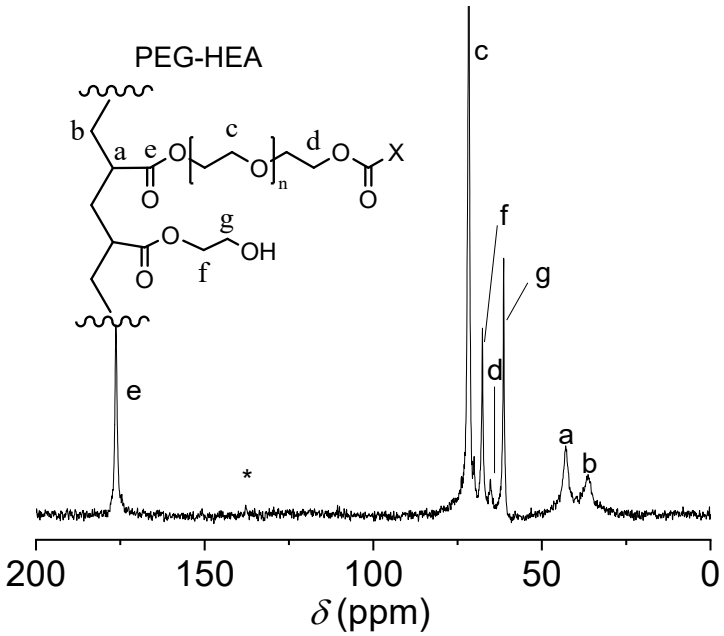

Figure S3. ^{13}C CPMAS NMR spectrum for cured PEG-HEA network and its assignment. Rotor spinning speed 12 kHz, contact time 10 ms, recycle delay 5s. * represents uncured acrylate double-bond carbon species.

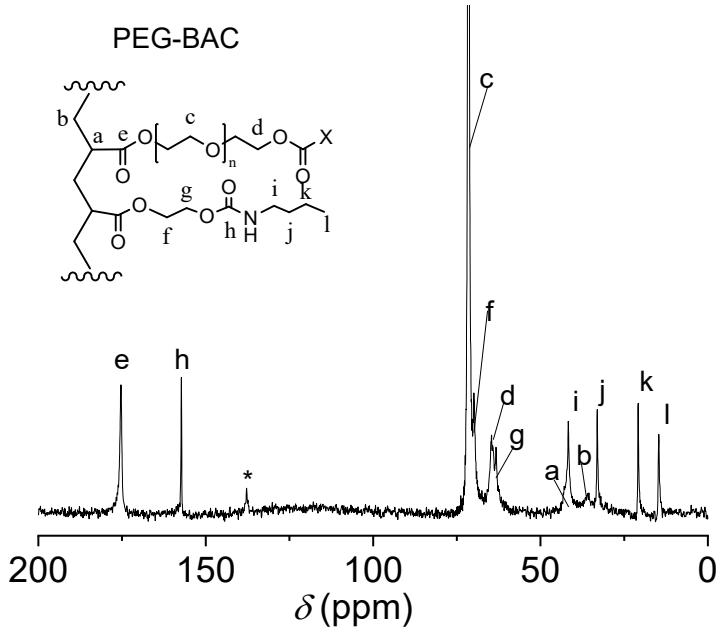

Figure S4. ^{13}C CPMAS NMR spectrum for cured PEG-BAC network and its assignment. Rotor spinning speed 12 kHz, contact time 10 ms, recycle delay 5s.* represents uncured acrylate double-bond carbon species.

S2. Chromatographic Analyses

The microwave-assisted hydrolysis of the UV-cured polymers (0.2 g) in 20 ml NaOH solution (1M, 48h) was performed in a Biotage® Initiator + microwave reactor. After hydrolysis, a solid silicate remained which originates from the glass flask (confirmed by IR). The liquid phase contained no ester (<2%), determined by IR after samples clean-up, indicating complete hydrolysis (>98%) under the conditions used.

The concentration of polyacrylic acid, PAA, and molecular weight distribution of the hydrolysates were determined using Size Exclusion Chromatography (SEC). These separations were performed with highly polar hydroxylated methacrylate Suprema columns: 2 times 8 mm × 300 mm pore size 1000 Å, coupled with an 8 mm × 300 mm pore size 100 Å column (all columns contain 10 µm particles), resulting in a separation range of 1–1000 kDa (PSS, Germany). The mobile phase (0.15 M NaCl, 0.08 M Tris (Tris(hydroxymethyl)aminomethane)), pH 8.0) was pumped at a flow rate of 1.0 mL/min. The SEC experiments were performed on a Viscotek GPC Max (VE2001 GPC solvent/sample module, Sysmex, The Netherlands) coupled to a Viscotek TDA 302 triple detector array (Sysmex, The Netherlands). The hydrolysates (samples) were centrifuged for 30 minutes (Ministar, VWR, The Netherlands), the clear upper layer was transferred to a vial, and injected (100 µL).

The concentration of PEG was determined using liquid chromatography (LC) coupled to CAD (Charged Aerosol Detector, quantification) and TOF-MS detection (qualification). The LC experiments were performed using an Ultimate 3000 LC (Dionex, The Netherlands), equipped with a terniary pump, autosampler, column department, coupled to a Charged Aerosol Detector (Corona Plus, ESA) and a Time-Of-Flight mass-spectrometer (TOF-MS, MicrOTOF, Bruker, Germany). The MS was run in positive mode with the following conditions: m/z range 50-3000, positive mode, capillary voltage 4500V, dry gas flow 7 L N_2/min, nebulizer pressure 2 bar, dry temperature 220ºC. The LC-CAD-MS system was controlled using DCMS link software (version 6.80 build 2214 (Dionex, The Netherlands). The LC separation was performed using a 3.0*150 mm BEH C18 column (2.5 µm particle size) (Waters, Germany) operating at 40°C. The flow rate was 0.5 ml/min. A gradient of water (0.1% formic acid) to acetonitrile was used; t = 0 min with 100% (v/v) water (0.1% formic acid), stayed there for 1 min and changed then to 100% (v/v) acetonitrile at t = 34 min for 1 min (stop time = 45 min). The injection volume is 5 µL. A 5-point

external calibration curve was established using a narrow PEG standard (Agilent, Mp 800 g/mol) in water. CAD detection was used for quantitation purposes; a cubic fit was used to establish the calibration curve.

All solvents and reagents used (acetonitrile, $CHCl_3$, formic acid, sodium chloride (NaCl), Tris and PEG were of p.a. quality (Merck, Darmstadt, Germany), ultra-pure water was obtained using a ELGA Purelab Ultra system (VWR, The Netherlands). All results are summarized in Table S1.

Sample No.	Monomer Type	$w\%_{PEGDA}$ (%)	PAA					PEG
			M_w (kDa)	M_n (kDa)	PDI	Conc. (mg/kg)	n (PAA)	Conc. (mg/kg)
1	HEA	90	21.0	9.5	2.2	2012	131	2280
2	HEA	70	22.1	10.5	2.1	2564	146	2210
3	HEA	50	29.5	11.8	2.5	2885	164	1910
4	HEA	30	28.1	12.7	2.2	3025	177	1580
5	HEA	10	29.5	11.3	2.6	3335	157	1020
6	BAC	90	24.6	11.2	2.2	1854	155	2300
7	BAC	70	27.6	10.2	2.7	2545	142	2120
8	BAC	50	25.6	12.8	2.0	2324	178	2040
9	BAC	30	29.8	11.5	2.6	2954	160	1640
10	BAC	10	20.8	9.9	2.1	3254	138	1040

Table S1. Weight average molecular weight (M_w), number average molecular weight (M_n) and PDI of PAA after hydrolysis of the UV-cured acrylate networks. Also the concentrations of both PAA and PEG after hydrolysis of the UV-cured acrylate networks, as determined by SEC and LC analysis. Note Samples 1-10 are the same as in Table 2 (labelled there the w%MA).

S3. NMR Analyses of H-bonding

As shown in Fig. S6, the presence of hydrogen bonding can be assessed by variable temperature ^{1}H NMR spectroscopy as the OH (NH) chemical shift change significantly upon increasing the temperature.[2, 3] In Fig. S7 the changes in chemical shifts on varying the sample temperature are shown. For non-hydrogen bonding groups (e.g. the -CH_2- group in PEG) temperature had little effect on either the chemical shift. When hydrogen bonding groups are present, on increasing the temperature the $\delta(^1H)$ for both –OH group in PEG-HEA and –NH group in PEG-BAC shifted to higher field. These changes can be explained as arising from the dynamics of H-bonding exchange.[4] Normally, such groups are in equilibrium between bonding and non-bonding states; at room temperature this exchange is usually relatively fast on the NMR time scale, therefore an averaged $\delta(^1H)$ for the two states is observed. On increasing the temperature the bound state population decreases and the exchange rate increases resulting in a decrease in chemical shift. These changes are consistent with previous studies in which bonds formed from –OH groups are found to be stronger than those from –NH groups.[5]

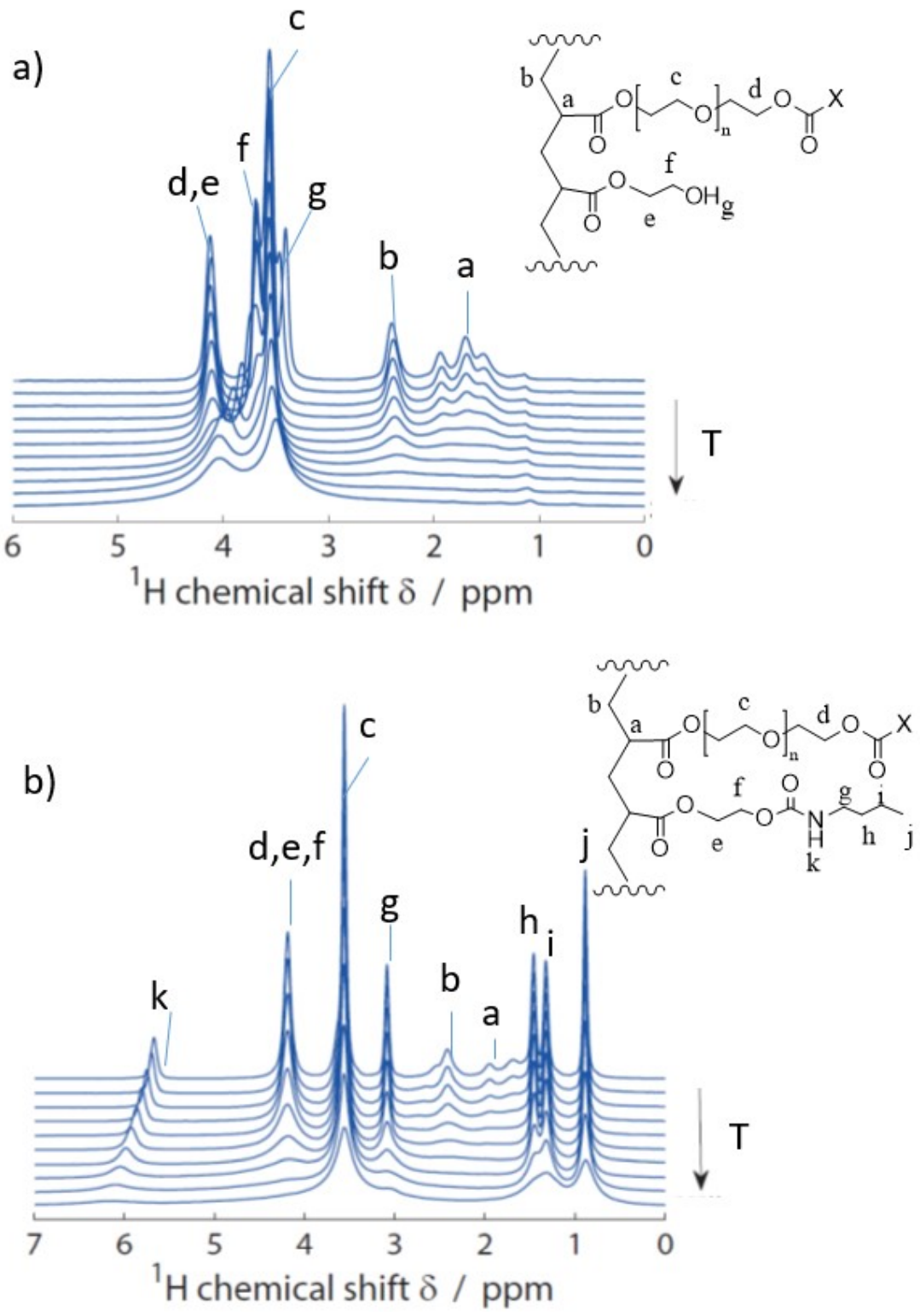

Figure S5. NMR spectra of a) PEG-HEA network (50w% HEA) b) PEG-BAC (50w% BAC) at different temperatures from 297 to 397 K. Larmor Frequency 600 MHz, rotor frequency 12 kHz, recycle delay 5 s (insert: NMR chemical shift assignment for these networks).

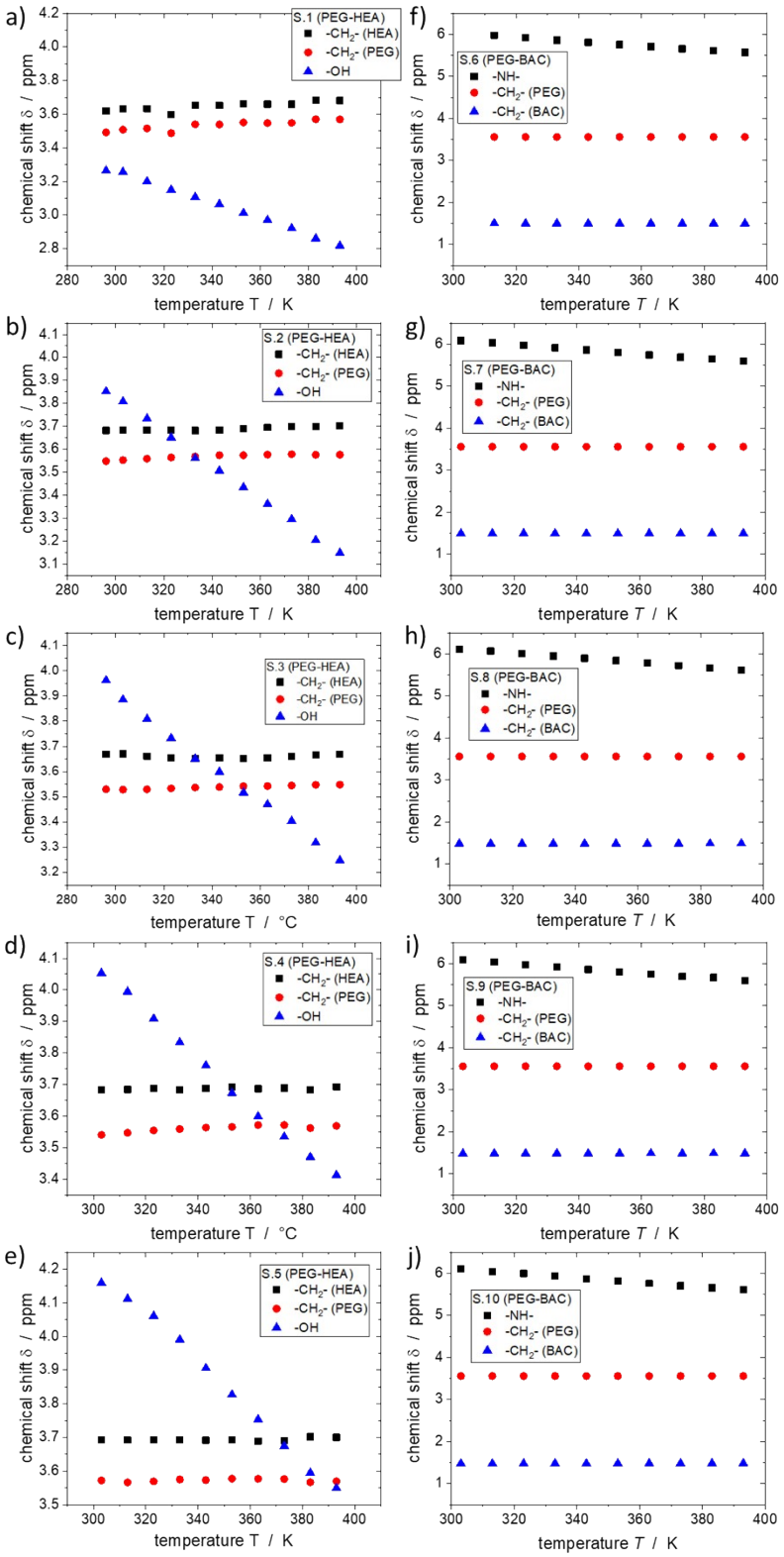

Figure S6. Temperature dependence of the ^{1}H NMR chemical shifts for the all the networks; (a-e) PEG-HEA, (f-j) PEG-BAC. The response of the PEG unit, copolymer unit and -OH/-NH groups are included for comparison.

S4. Dynamic Mechanic Analyses

According to classical rubber elasticity theory, the mean molar mass of network chains between chemical crosslinks and trapped chain entanglements, M_{c+e}, can be calculated using rubber elasticity theory

$$M_{c+e} = 3\rho RT(1-x)/E' \quad \text{(S1)}$$

where ρ is the specific density measured for individual sample, R is the gas constant (8.31 J/(mol·K)), T is the absolute temperature and x is the volume fraction of side chain fragment of monoacrylate. Hence the decrease of E' in the rubbery plateau with increasing monoacrylate content is consistent with an increase in M_{c+e} due to decreasing network crosslink density as we observed previously for PEG-700 hexyl-acrylate networks.[4]

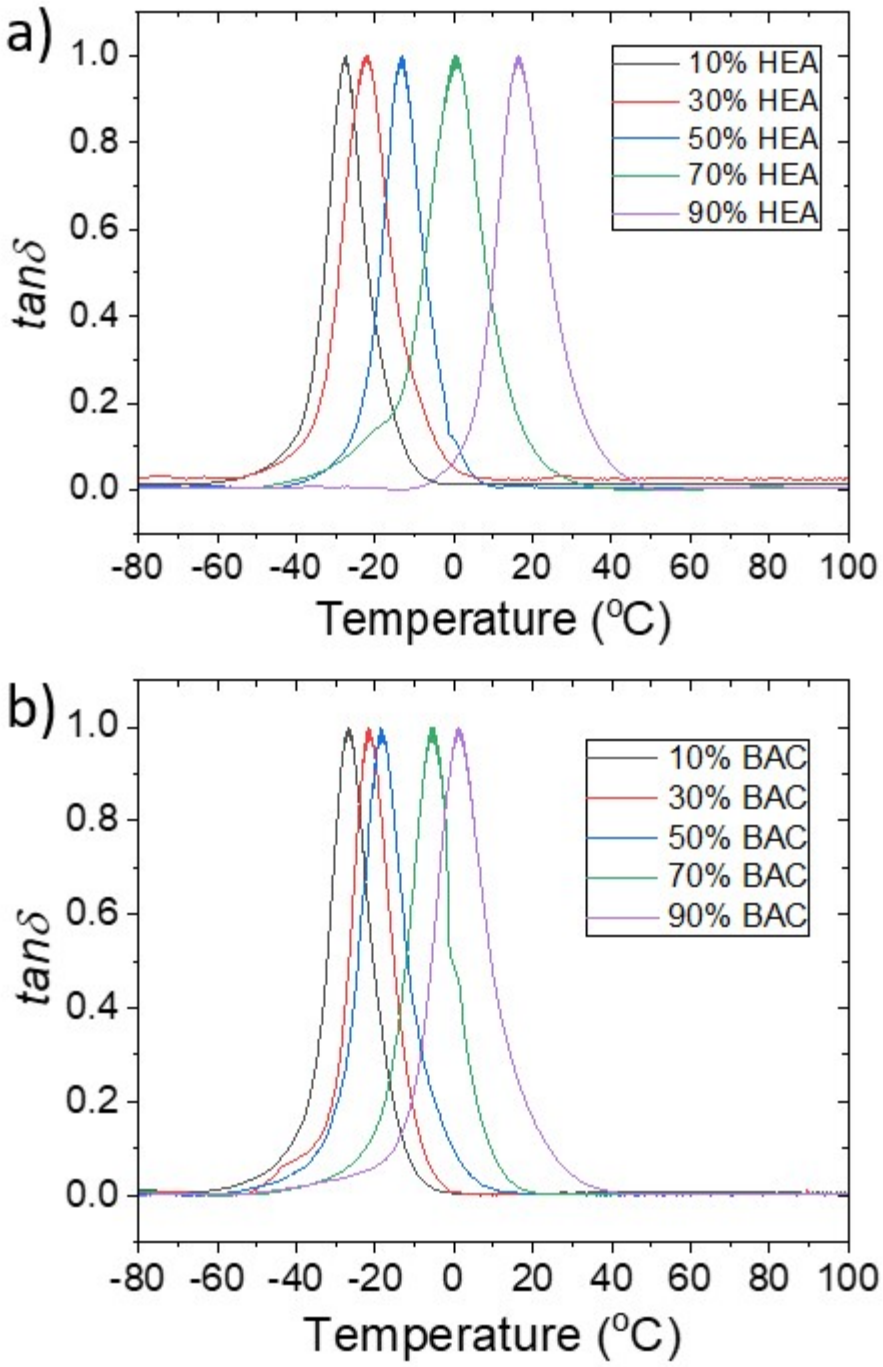

+

Figure S7. Ratio between storage modulus and loss modulus analyses ($tan(\delta)$) of all the samples (a) PEG-HEA series, (b) PEG-BAC series.

In polymer physics, the Flory–Fox equation is a simple empirical formula that relates molecular weight to the glass transition temperature of a polymer system. As an alternative equation to Flory-Fox equation used for polyacrylates, the Fox-Loshaek equation, usually applied to homogeneous polymer systems, is given by[6]:

$$T_g = T_g^{\infty} - K/M_c$$

where T_g^{∞} is the T_g of a polymer of infinite mol. wt., and K is a material constant, M_c is molecular weight of network chain.

S5. ^{1}H NMR T_2 Relaxation Analyses

The ^{1}H transverse magnetization relaxation (T_2 relaxation) times of these networks were measured on Bruker Minispec MQ20 spectrometer operating at 20 MHz. The T_2 relaxation decay was measured with the Hahn-echo (HE) pulse sequence, 90^o_x—τ_{HE}—180^o_y—τ_{HE}—(acquisition), where $\tau_{HE} \geq 35$ μs. An echo signal is formed after the second pulse in the HE with a maximum at time $t = 2\tau_{HE}$ after the first 90° pulse. By varying τ_{HE}, the amplitude of the transverse magnetization, $A(t)$, is measured as a function of time t. The resulting decay curve of the transverse magnetization then were fitted with a linear combination of Weibull functions as described in the previous work[7]:

$$A(t) = A_1(0) f_W(\alpha_1)\left[-\left(\frac{t}{T_{2,1}}\right)\right] + A_2(0) f_W(\alpha_2)\left[-\left(\frac{t}{T_{2,2}}\right)\right] + A_3(0) f_W(\alpha_3)\left[-\left(\frac{t}{T_{2,3}}\right)\right] \quad (S2)$$

It should be noted that the complex shape of T_2 decay is caused by several reasons, i.e., the complex origin of the transverse magnetization relaxation of polymer networks[8, 9], the presence of network defects, and different averaging of dipole-dipole interactions for polymer chains composed of different chain segments like the one in this study. The Weibull function is commonly used for describing the relaxation of polymers with restricted and heterogeneous molecular mobility. Unlike Gaussian or Abragamian functions[10], which are used to describe strongly restricted mobility including crystalline lattice, Weibull function, as a compressed exponential function, gives a better description of more isotropic dynamics for polymers well above T_g.

The population average transverse relaxation time $T_{2,av}$, was calculated as $T_{2,av} = 1/\left(\sum_{i=1}^{n} A_i(0)/T_{2,i}\right)$. $T_{2,av}$ value will be used below for calculating the molecular mass of network chains. It is worth noting that the amount of defects (typically have long relaxation time) have been found below 3% across all the samples, hence, the impact of defects on the overall network behavior can be negligible.

T_2 relaxation decays were measured for dry gels, as well as for swollen ones at different swelling degrees. Deuterated 1,1,2,2-$C_2D_2Cl_4$ was used as the solvent for swelling. After adding the solvent,

samples were stored in NMR tubes at room temperature in the dark environment for 1 day for equilibration.

The ^{1}H NMR T_2 relaxation experiments in this study were performed at 70^{o}C, well above the T_g value of the gels. It is known the T_2 relaxation time for rubbery materials is very sensitive to the conformational mean position of network chains at temperatures well above T_g. At these temperatures, T_2 value for polymer networks without defects does not depend on temperature and can be used for calculating weight average molar mass of network chains[11]

This calculation is based on the quantitative correlation between the T_2 value at high temperature plateau and the number of statistical segments in the network chains. For polymers containing aliphatic protons in the main chain, we have shown[1, 11] that is also possible to estimate apparent M_{c+e} values from the T_2 values using the following relation.

$$M_{c+e} = \frac{T_2^p C_\infty M_u}{\alpha T_2^{rl} n} \qquad (S3)$$

where α is a theoretical coefficient which depends on the angle between the segment axis and the inter-nuclear vector of the nearest nuclear spins on the main chain. For polymers containing aliphatic protons in the main chain, the coefficient α is close to 6.223. The T_2^{rl} value is related to the strength of intra-chain ^{1}H-^{1}H interactions in the rigid lattice. Here we use 8.5 μs corresponding to the value measured at 108 K. M_u is the molar mass per elementary chain unit, and n is the number of backbone bonds in an elementary chain unit. C_∞ is the number of backbone bonds in the statistical segment, a mean value of 5.0 is used in this study. The T_2^p is the T_2 value at the high temperature plateau, which is measured in this study.

S6. Double Quantum NMR Analyses

In the DQ experiment two sets of data, a DQ build-up curve, I_{DQ}, dominated by dipolar coupled segments of the polymer network and a reference intensity decay curve, I_{ref}, are recorded with varied DQ evolution time, τ_{DQ}, which is incremented in terms of full rotor periods, N_{τ_R} in the BaBa experiment. The two signal functions are subject to relaxation effects due to intermediate motions and pulse sequence imperfections. In order to obtain structure information independently of the latter the data is normalize by a point-by-point division of the DQ build-up by the sum relaxation function, $I_{\Sigma MQ} = I_{DQ} + I_{ref}$. The normalized DQ build-up function, $I_{nDQ} = I_{DQ}/(I_{\Sigma MQ} - tails)$, is corrected for the possible contribution of slowly relaxing, exponential signal tails in I_{ref} (these are attributed to non-coupled spins, i.e., network defects). Hence I_{nDQ} exclusively reflects residual dipolar interactions that are related to the network contribution to the residual dipolar couplings, D_{res}, which can be obtained by fitting I_{nDQ} to an appropriate function [12, 13]. For a quantitative picture of the coupling constant distribution, $p(D_{res})$, the data is evaluated with an optimized numerical procedure (*ftikreg*) [13]. The resulting $p(D_{res})$ function reliably yield the average residual dipolar coupling constant, D_{avg}, and its standard deviation σ. The D_{avg} value is directly proportional to the cross-link density while the dimensionless relative distribution width, $\sigma_{rel} = \sigma/D_{res}$ gives information about the spatial distribution of cross-links and its distribution of anisotropy of segmental motions, and thus the network heterogeneity and network defects.

Note that the rather complex spin system of PEG-HEA and PEG-BAC copolymer networks prevents the direct calculation of order parameters. Thus, the D_{avg} values of the individual chemical groups within a network cannot be compared with each other. The analysis is restricted to the relative distribution width, σ_{rel}, and the relative changes of the individual D_{avg} value for the different network samples.

MA wt%	PEG-HEA Samples		PEG-BAC Samples	
	$D_{res}/2\pi$ (kHz)	$\sigma/2\pi$ (kHz)	$D_{res}/2\pi$ (kHz)	$\sigma/2\pi$ (kHz)
10	2.26	1.68	2.20	1.88
30	1.83	1.01	1.71	0.99
50	1.51	0.88	1.43	0.81

70	0.99	0.42	0.89	0.51
90	0.43	0.25	0.42	0.24

Table S2. Relevant D_{res} and σ value obtained in this study.

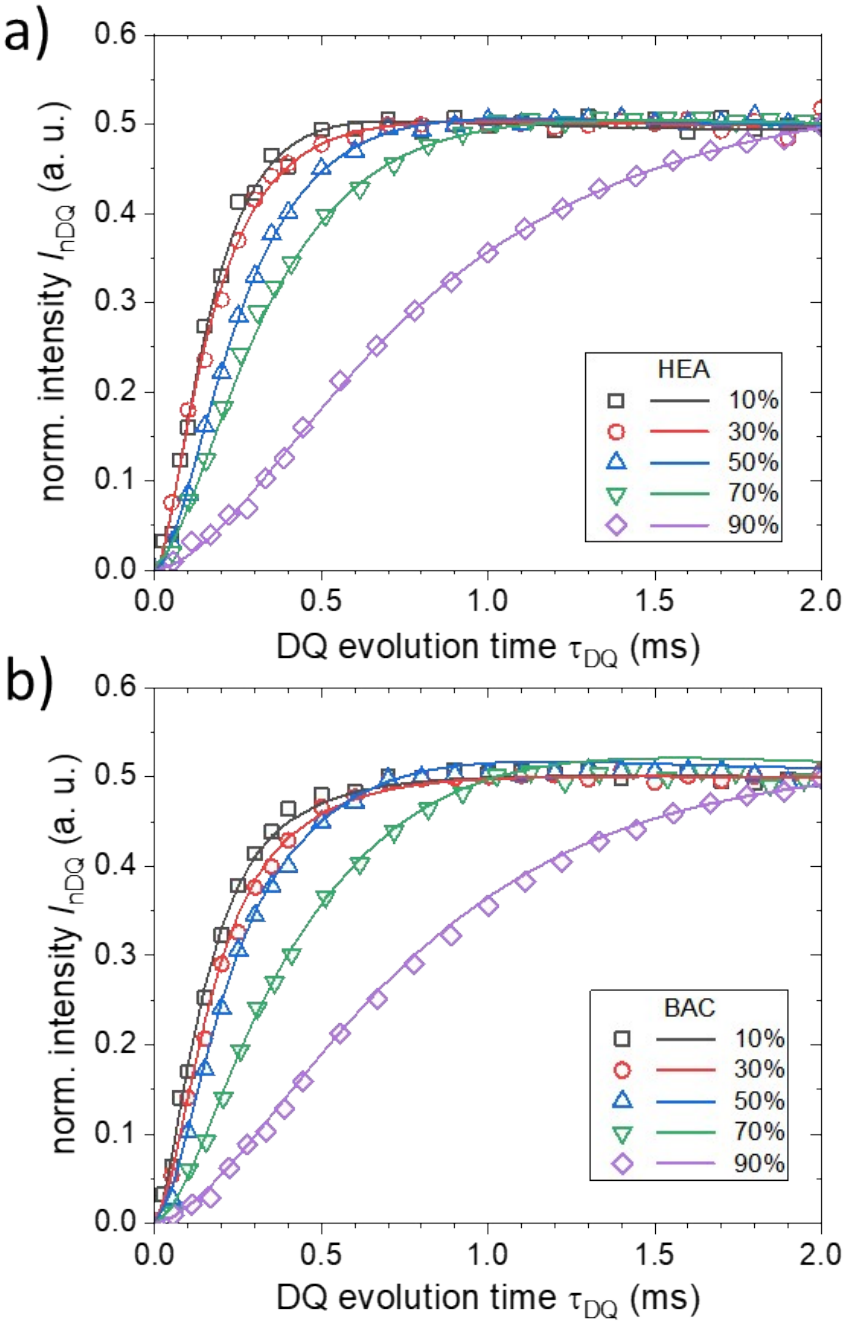

Figure S8. Normalized DQ build-up intensities of PEG chains (δ=3.56 ppm) for (a) PEG-HEA networks; (b) PEG-BAC networks. Points represent experimental data and solid lines are results of the numerical regularization fit obtained using *ftikreg*.

S7. Alfrey-Price $Q-e$ scheme analyses of copolymerization kinetics

To evaluate the potential for differences in kinetic preference for homo-polymerization in HEA and BAC, the reactivity ratios r_1 (for monoacrylate) and r_2 (for PEGDA) for all the components (HA, HEA, BAC and PEGDA) studied were estimated using the Alfrey-Price $Q-e$ scheme.[14] In this approach Q is a measure of reactivity arising from resonance stabilization, while e is a measure of polarity of the monomer due to the effect of the different functional groups on the vinyl group.[15] The Q and e values used in this study for HA/HEA/BAC (monomer 1), and for PEGDA (monomer 2) are shown in Table S3. Not all Q and e values are available, so the values for 2-ethylhexyl acrylate and acrylamide were used for HA and BAC[16, 17], respectively. In addition free and pendant double bonds are assumed to have equal reactivity in these calculations, an assumption which is less likely to be valid at extremely low and high levels of conversion.[18] Hence the outcome of the calculation should be viewed as indicative only.

Table S3. Reference Q, e values for monomers used in this study, and the calculated reactivity ratios r in the corresponding copolymerization process.

Monomer 1	Q_1	e_1	r_1	Monomer 2	Q_2	e_2	r_2
HA	0.37	+0.24	0.99	PEGDA	0.48	+1.28	0.34
HEA	0.75	+0.65	2.35	PEGDA	0.48	+1.28	0.29
BAC	0.23	+0.54	0.72	PEGDA	0.48	+1.28	0.81

The reactivity ratio r, which is the ratio between the rate constants k_{11} (homo-polymerization of species 1) and k_{12} (copolymerization between species 1 and 2) can be estimated as following, with the resulting values given in Table S3;

$$r_1 = Q_1 \frac{\exp\left(-e_1(e_1-e_2)\right)}{Q_2} \qquad (S4)$$

$$r_2 = Q_2 \frac{\exp\left(-e_2(e_2-e_1)\right)}{Q_1} \qquad (S5)$$

This approach implies a stronger preference for HEA to homo-polymerize than to copolymerize with PEGDA, and a preference of random copolymerization for PEG-HA and PEG-BAC. This also suggests the possibility of a strong kinetic driving force for formation of H-bonding clusters

in PEG-HEA, which is in addition to any thermodynamic preference (pre-organization). For PEG-BAC the kinetic effect is weaker. However, interestingly, the curing induced shift to higher wavenumber observed in the IR for the ν(N-H) modes suggests that even in PEG-BAC kinetics still dominate.

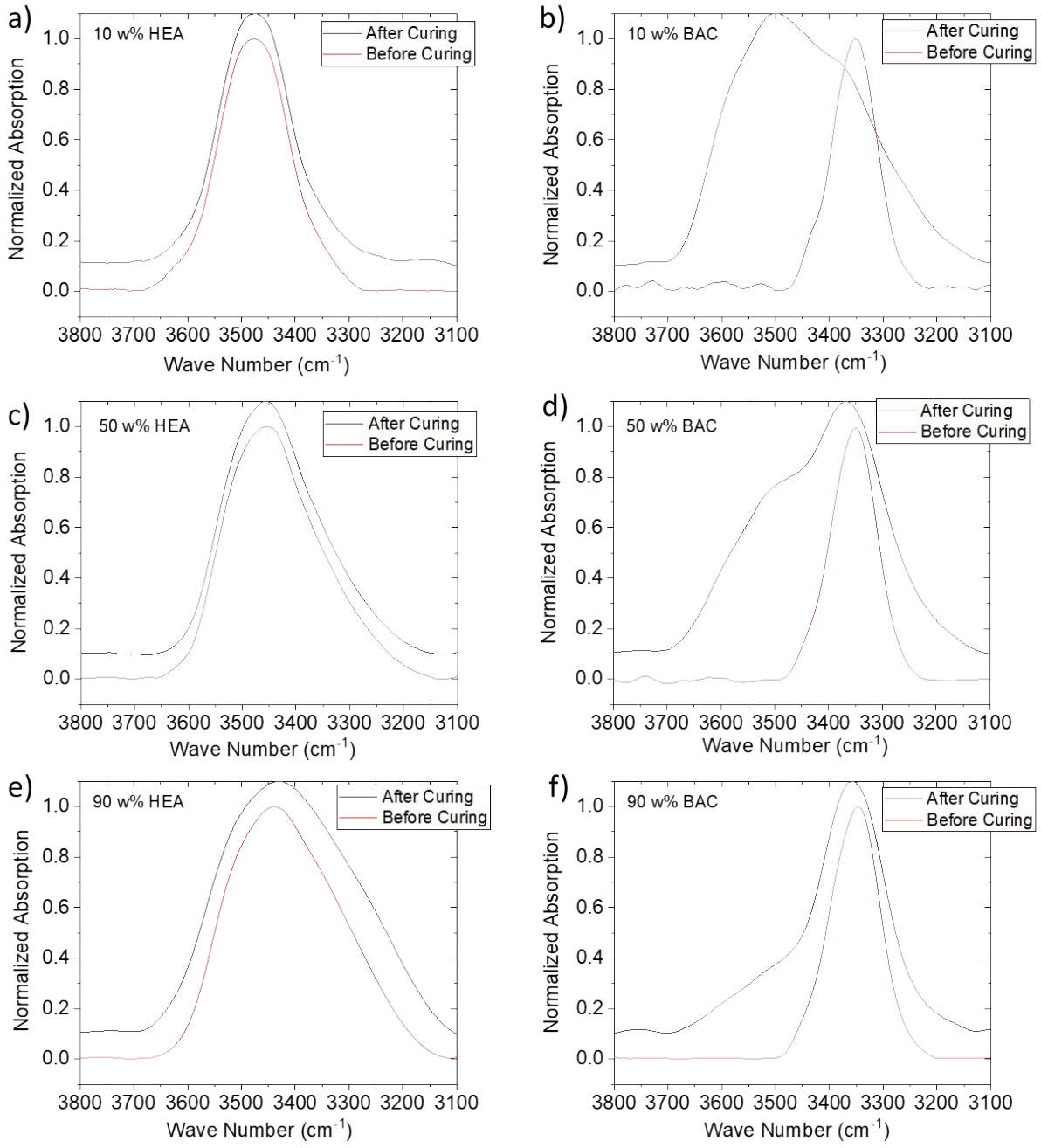

Figure S9. IR spectra of O-H/N-H stretching band from 3100-3800 cm^{-1} for (a) sample 1 (PEG-HEA: 10w% HEA); (b) sample 6 (PEG-BAC: 10w% BAC); (a) sample 3 (PEG-HEA: 50w% HEA); (a) sample 8 (PEG-BAC: 50w% BAC); (a) sample 5 (PEG-HEA: 90w% HEA); (a) sample 10 (PEG-BAC: 90w% BAC). The spectra were normalized by scaling the spectra by the maximum absorbance recorded in this region.

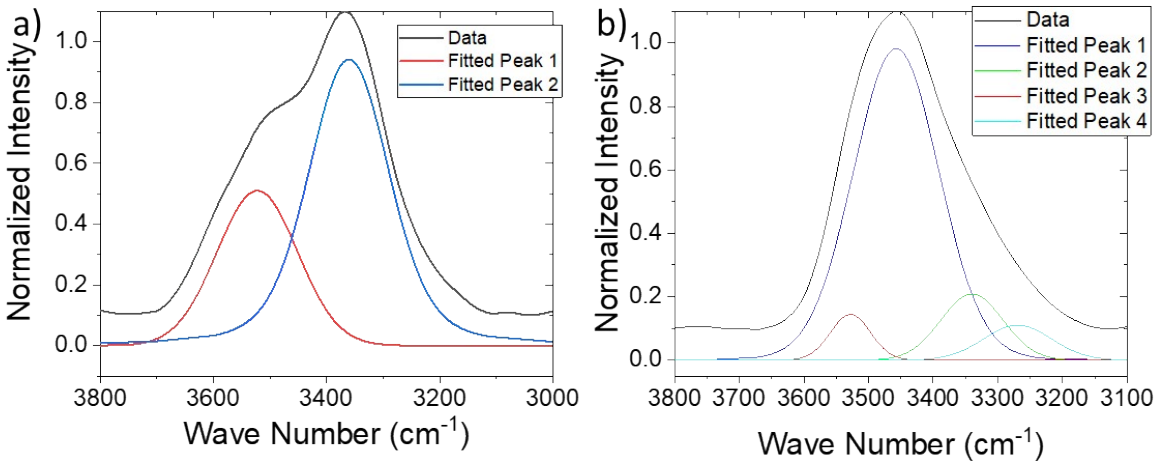

Figure S10. Example of deconvolution of IR spectra (a) sample PEG-BAC 50%, b) sample PEG-HEA 50%), red peak is for non-H-bonded, blue peak for H-bonded, green/cyan peak for different H-bonding mode in PEG-HEA samples.

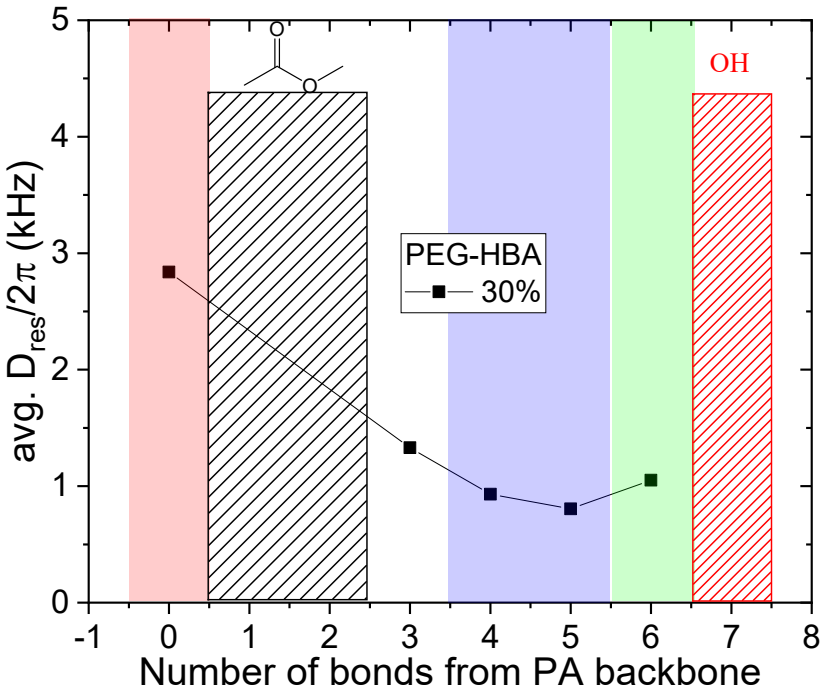

Figure S11. The $^{D_{avg}}$ values of chemical groups along the HBA (4-hydroxybutyl acrylate) side-chain in the PEG-HBA ($w^{\%_{HBA}}$ 30) network

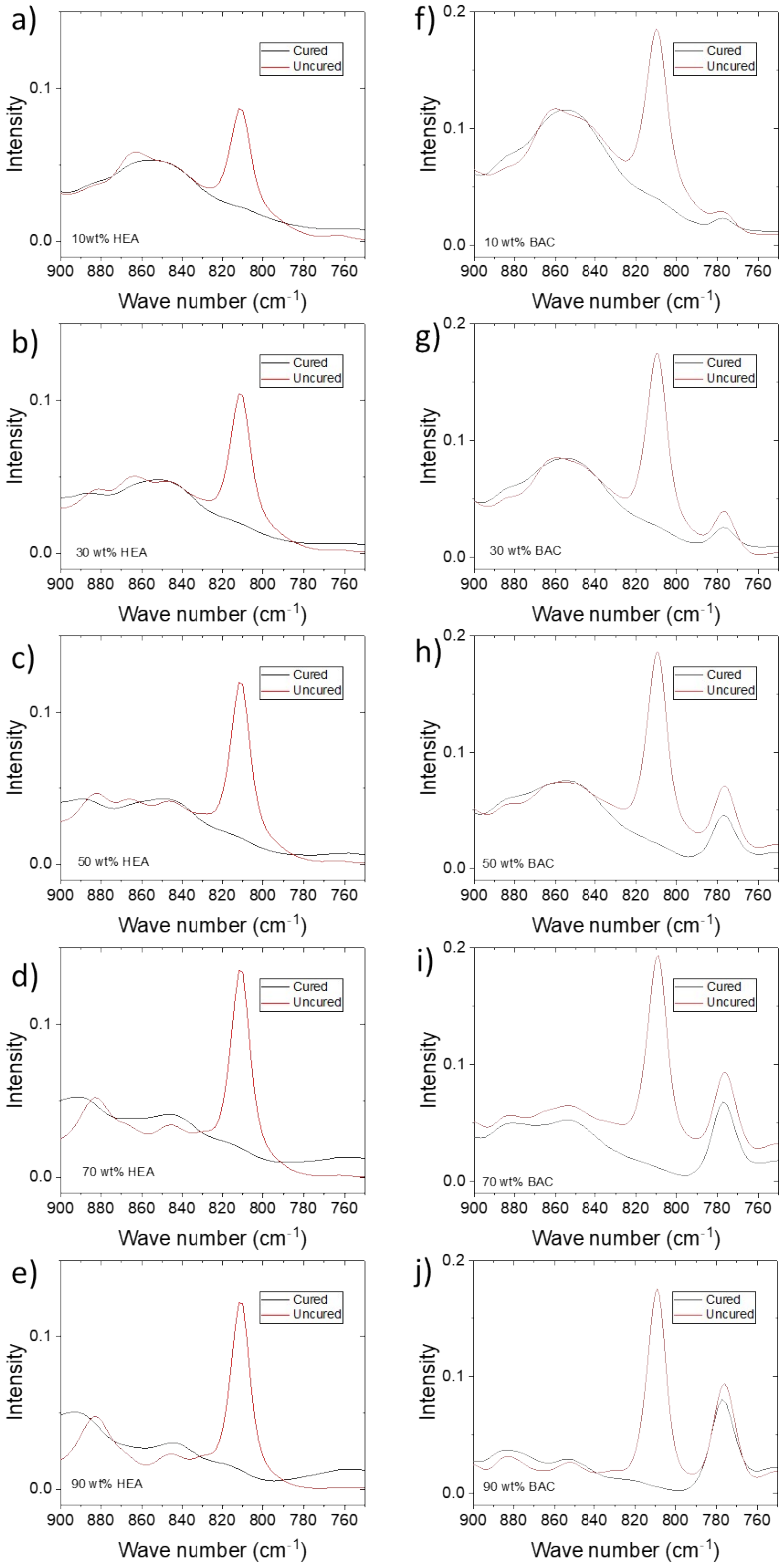

Figure S12. IR spectra of acrylate C-H deformation band at 810 cm^{-1} for uncured and cured PEG-HEA (a-e) and PEG-BAC (f-j)

References

1. B. Wu, W. Chasse, R. Peters, T. Brooijmans, A. A. Dias, A. Heise, C. J. Duxbury, A. P. M. Kentgens, D. F. Brougham and V. M. Litvinov, Network Structure in Acrylate Systems: Effect of Junction Topology on Cross-Link Density and Macroscopic Gel Properties, *Macromolecules*, 2016, **49**, 6531-6540.
2. T. G. Pedersen, B. W. Sigurskjold, K. V. Andersen, M. Kjaer, F. M. Poulsen, C. M. Dobson and C. Redfield, A Nuclear-Magnetic-Resonance Study of the Hydrogen-Exchange Behavior of Lysozyme in Crystals and Solution, *J Mol Biol*, 1991, **218**, 413-426.
3. S. H. Gellman, G. P. Dado, G. B. Liang and B. R. Adams, Conformation-Directing Effects of a Single Intramolecular Amide-Amide Hydrogen-Bond - Variable-Temperature Nmr and Ir Studies on a Homologous Diamide Series, *J Am Chem Soc*, 1991, **113**, 1164-1173.
4. S. Scheiner, *Hydrogen bonding a theoretical perspective*, Oxford University Press, New York etc., 1997.
5. G. A. Jeffrey, *An introduction to hydrogen bonding*, Oxford University Press, New York, 1997.
6. T. G. Fox and S. Loshaek, Influence of Molecular Weight and Degree of Crosslinking on the Specific Volume and Glass Temperature of Polymers, *J Polym Sci*, 1955, **15**, 371-390.
7. V. M. Litvinov, EPDM/PP thermoplastic vulcanizates as studied by proton NMR relaxation: Phase composition, molecular mobility, network structure in the rubbery phase, and network heterogeneity, *Macromolecules*, 2006, **39**, 8727-8741.
8. M. G. Brereton, Nmr Transverse Relaxation Function Calculated for Constrained Polymer-Chains - Application to Entanglements and Networks, *Macromolecules*, 1990, **23**, 1119-1131.
9. V. M. Litvinov, M. E. Ries, T. W. Baughman, A. Henke and P. P. Madoka, Chain Entanglements in Polyethylene Melts. Why Is It Studied Again?, *Macromolecules*, 2013, **46**, 541-547.
10. D. Besghini, M. Mauri and R. Simonutti, Time Domain NMR in Polymer Science: From the Laboratory to the Industry, *Appl Sci-Basel*, 2019, **9**.
11. V. M. Litvinov and A. A. Dias, Analysis of network structure of UV-cured acrylates by H-1 NMR relaxation, C-13 NMR spectroscopy, and dynamic mechanical experiments, *Macromolecules*, 2001, **34**, 4051-4060.
12. K. Saalwachter, F. Lange, K. Matyjaszewski, C. F. Huang and R. Graf, BaBa-xy16: Robust and broadband homonuclear DQ recoupling for applications in rigid and soft solids up to the highest MAS frequencies, *J Magn Reson*, 2011, **212**, 204-215.
13. W. Chasse, J. L. Valentin, G. D. Genesky, C. Cohen and K. Saalwachter, Precise dipolar coupling constant distribution analysis in proton multiple-quantum NMR of elastomers, *J Chem Phys*, 2011, **134**.
14. T. Alfrey Jr and C. C. Price, Relative reactivities in vinyl copolymerization, *J Polym Sci*, 1947, **2**, 101-106.
15. G. G. Odian, *Principles of polymerization*, Wiley-Interscience, Hoboken, N.J., 4th edn., 2004.
16. R. Z. Greenley, Q and e Values for Free Radical Copolymerizations of Vinyl Monomers and Telogens, *The Wiley Database of Polymer Properties,* 2002.
17. J. Brandrup, E. H. Immergut and E. A. Grulke, *Polymer handbook, 4th edition*, Wiley, New York ; Chichester, 4th edn., 2004.
18. J. G. Kloosterboer, G. F. C. M. Lijten and H. M. J. Boots, Network Formation by Chain Crosslinking Photopolymerization and Some Applications in Electronics, *Makromol Chem-M Symp*, 1989, **24**, 223-230.